*Journal of Applied Mechanics and Technical Physics, Vol. 43, No. 1, pp. 120–127, 2002*

# EFFECT OF HEAT FLOW ON HEAT-TRANSFER CHARACTERISTICS FOR A SUPERSONIC SPATIAL FLOW AROUND A SPHERICALLY BLUNTED CONE

**V. I. Zinchenko and A. Ya. Kuzin**

UDC 536.24.01

*Heat-transfer processes for a supersonic spatial flow around a spherically blunted cone were studied by solving direct and inverse three-dimensional problems taking into account heat flow along the longitudinal and circumferential coordinates. It is shown that highly heat-conducting materials can be used to advantage to decrease the maximum temperatures on the windward side of streamline bodies.*

In [1–7], it was shown that the use of highly heat-conducting materials and injection in supersonic flight vehicles provides for a decrease in surface temperature in the region of high thermal loads. The more and more stringent requirements on the accuracy in determining heat-transfer characteristics necessitate the improvement of mathematical models and methods for calculating heat- and mass-transfer processes in gas and solid phases [8] and the development of other methods for heat-transfer calculations, such as methods for solving inverse problems (IP) [9]. Solutions of IP allow one to control and refine the solution of the conjugate problem and to reduce the calculation time. In addition, they are irreplaceable when the only available experimental information is the temperature at some points or on a part of the shell of a streamline body [6, 7]. However, the ill-posedness of IP of heat transfer [9] complicates their solution because in this case, one needs to develop and use a special regularizing algorithm. The difficulties of solution increase considerably for non-one-dimensional IP. At the same time, the use of combined methods of thermal protection based on the simultaneous employment of highly heat-conducting materials and gas injection leads to the necessity of developing appropriate methods for solving multidimensional IP.

The effect of heat flow on heat-transfer characteristics was investigated for axisymmetric flow [1–3, 6, 7] and for motion at incidence [4, 5]. In the last case, heat flow occurs not only along the longitudinal but also along the circumferential coordinate because of the large difference in heat-transfer rate between the windward and leeward sides. Therefore, to correctly consider heat-transfer processes, it is necessary to use three-dimensional formulations of the direct and inverse problems [10].

In the present paper, considering the problem of heating of the shell of a spherically blunted cone in a supersonic spatial high-enthalpy airflow in a full mathematical formulation, we discuss algorithms and results of solution of direct and inverse three-dimensional heat-transfer problems. In the IP, the initial experimental information is the temperature on the rear surface of the shell as a function of the longitudinal and circumferential coordinates and time. We study the effect of heat flow along the longitudinal and circumferential coordinates on heat-transfer characteristics and limits of applicability of the solution of the IP in the one- and two-dimensional formulations for various materials of the shell.

**1. Physical and Mathematical Formulation of Direct and Inverse Problems.** We consider the heating of a spherically blunted cone in a supersonic airflow at incidence (Fig. 1). In regions I and II, heat transfer is described by heat-conduction equations in a natural system of coordinates attached to the body surface (the coordinate origin is at the point of intersection of the body symmetry axis with the surface):

Institute of Applied Mathematics and Mechanics, Tomsk State University, Tomsk 634050. Translated from Prikladnaya Mekhanika i Tekhnicheskaya Fizika, Vol. 43, No. 1, pp. 144–152, January–February, 2002. Original article submitted June 6, 2001; revision submitted August 29, 2001.

 0021-8944/02/4301-0120 $27.00 

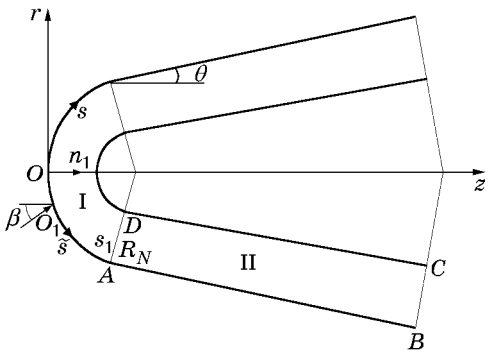


Fig. 1

$$\rho c\,\frac{\partial T}{\partial t} = \frac{1}{Hr}\Big[\frac{\partial}{\partial n_1}\Big(Hr\lambda\,\frac{\partial T}{\partial n_1}\Big) + \frac{\partial}{\partial s}\Big(\frac{r\lambda}{H}\,\frac{\partial T}{\partial s}\Big) + \frac{\partial}{\partial \eta}\Big(\frac{H}{r}\,\lambda\,\frac{\partial T}{\partial \eta}\Big)\Big], \tag{1.1}$$

$$0 < n_1 < L, \quad 0 < s < s_B, \quad 0 < \eta < \pi, \quad 0 < t \leqslant t_{\text{fin}}.$$

The initial and boundary conditions are

$$T\Big|_{t=0} = T_n; \tag{1.2}$$

$$q_w - \varepsilon\sigma T_w^4 = -\lambda\,\frac{\partial T}{\partial n_1}\Big|_w, \qquad 0 \leqslant s \leqslant s_B; \tag{1.3}$$

$$\frac{\partial T}{\partial n_1}\Big|_L = 0, \qquad 0 \leqslant s \leqslant s_C, \tag{1.4}$$

condition on line BC is

$$\frac{\partial T}{\partial s} = 0, \tag{1.5}$$

and condition in the plane of symmetry is

$$\frac{\partial T}{\partial \eta}\Big|_{\eta=0} = \frac{\partial T}{\partial \eta}\Big|_{\eta=\pi} = 0. \tag{1.6}$$

For region I, $H = (R_N - n_1)/R_N$ and $r = (R_N - n_1)\sin\bar{s}$ and for region II, $H = 1$ and $r = (R_N - n_1)\cos\theta + (s - s_A)\sin\theta$. Here $\bar{s} = s/R_N$ and $s = s_A + \cos^{-1}\theta[z + (\sin\theta - 1)R_N]$.

The heat flux from the gas phase $q_w$ is given by the formulas of [11] for the spatial case with laminar and turbulent boundary-layer flows:

$$q_w = (\alpha/c_p)(h_r - h_w). \tag{1.7}$$

In a coordinate system attached to the stagnation point $O_1$, on the spherical part $0 \leqslant \tilde{s} \leqslant \tilde{s}_*$ for laminar boundary-layer flow, we have

$$\alpha/c_p = 1.05V_\infty^{1.08}(0.55 + 0.45\cos 2\tilde{s})/(R_N/\rho_\infty)^{0.5},$$
$$h_r = h_{e0}[(p_e/p_{e0})^{(\gamma-1)/\gamma} + (u_e/v_m)^2\mathrm{Pr}^{\,0.5}] \tag{1.8}$$

and for turbulent flow in the region $\tilde{s}_* < \tilde{s} < \tilde{s}_1$, we have

$$\alpha/c_p = 16.4V_\infty^{1.25}\rho_\infty^{0.8}(3.75\sin\tilde{s} - 3.5\sin^2\tilde{s})/[R_N^{0.2}(1 + h_w/h_{e0})^{2/3}],$$
$$h_r = h_{e0}[(p_e/p_{e0})^{(\gamma-1)/\gamma} + (u_e/v_m)^2\mathrm{Pr}^{\,1/3}]. \tag{1.9}$$

On the conical part of the body for turbulent flow in the region $\tilde{s}_1 \leqslant \tilde{s} \leqslant \tilde{s}_B$, we have

$$\alpha/c_p = 16.4V_\infty^{1.25}\rho_\infty^{0.8}2.2(p_e/p_{e0})(u_e/v_m)/[R_N^{0.2}(1 + h_w/h_{e0})^{2/3}k^{0.4}\bar{r}_{2w}^{0.2}]. \tag{1.10}$$

In (1.1)–(1.10), $t$ is time, $n_1$, $s$, and $\eta$ are the components of the natural coordinate system, $T$ is the temperature, $p$ is the pressure, $\rho$ is the true density, $c$ and $\lambda$ are the heat capacity and thermal conductivity, $h$ is the enthalpy,

$H$ and $r$ are the Lamé coefficients of cylindrical coordinates, $\alpha/c_p$ is the heat-transfer coefficient, $R_N$ is the radius of the spherical bluntness, $\sigma$ is the Stefan–Boltzmann constant, $\varepsilon$ is the emissivity of the surface of the streamlined material, $\tilde{s}_*$ is the coordinate of the point of instability in a coordinate system with origin at the stagnation point, $q_w$ is the convective heat flux from the gas phase, $\beta$ and $\theta$ are the angle of attack and the cone angle, respectively, Pr is the Prandtl number, $L$ is the thickness of the shell, $V_\infty$, $\rho_\infty$, and $\mathrm{M}_\infty$ are the free-stream velocity, density, and Mach number, $\gamma$ is the adiabatic exponent, $u_e/v_m = [1-(p_e/p_{e0})^{(\gamma-1)/\gamma}]^{0.5}$, $v_m = (2h_{e0})^{0.5}$, $h_{e0} = h_\infty[1+0.5(\gamma-1)\mathrm{M}_\infty^2]$, $h_w = b_1T_w + b_2T_w^2/2$, and $\tilde{s} = \arccos(\cos\bar{s}\cos\beta + \sin\bar{s}\sin\beta\cos\eta)$. The subscripts $e0$ and $w$ refer to the conditions at the stagnation point on the outer surface of the boundary layer and at the interface between the gas and solid phases, the subscript $\infty$ correspond to free-stream conditions, the subscripts in, fin, and asterisk denote the initial, final, and characteristic parameters, respectively, bar refers to dimensionless quantities, and $L$ to quantities on the inner surface of the shell.

The three-dimensional direct problem (DP) consists of determining the temperature $T(n_1, s, \eta, t)$ that satisfies Eq. (1.1) in the open region $D = \{(n_1, s, \eta, t)\colon 0 < n_1 < L,\ 0 < s < s_B,\ 0 < \eta < 2\pi,\ 0 < t \leqslant t_{\text{fin}}\}$ and the initial and boundary conditions (1.2)–(1.6) and that is continuous together with the derivative $\partial T(n_1, s, \eta, t)/\partial n_1$, $\partial T(n_1, s, \eta, t)/\partial s$, and $\partial T(n_1, s, \eta, t)/\partial\eta$ in the closed region $\bar{D}$. If the temperature $T(n_1, s, \eta, t)$ in the region $\bar{D}$ is unknown except on the boundary $n_1 = L$, and it is required to find its values, the convective heat flux $q_w(s, \eta, t)$ and the total heat flux $Q_w(s, \eta, t) = q_w(s, \eta, t) - \varepsilon\sigma T_w^4$ on the windward and leeward sides from the known initial condition (1.2), boundary condition (1.4)–(1.6), and the additional condition

$$T(L, s, \eta, t) = T_L^{\exp}(s, \eta, t), \tag{1.11}$$

the three-dimensional boundary-value IP is solved.

**2. Algorithms of Solution of the Direct and Inverse Problems.** The three-dimensional DP of heat transfer was solved by the method of splitting in the space variables $n_1$, $s$, and $\eta$ [12]. The one-dimensional heat-conduction equations obtained by splitting in each time layer were calculated by the integrointerpolation method (IIM) [13]. Because for motion of the body at incidence, the condition of symmetry at the point $s = 0$ is not satisfied, the temperature in the $s$ direction was calculated with a variable through step for the windward and leeward sides subject to the conditions of equal temperatures and heat fluxes at the point $s = 0$ ("joining" conditions). As a result, the circumferential coordinate $\eta$ changed in the range from 0 to $\pi/2$, and the temperature for the remaining values of $\eta$ was determined using the symmetry conditions at $\eta = 0$ and $\eta = \pi$, which reduced considerably the computing time. An advantage of the proposed algorithm of solution of the DP is its adaptability because the "joining" conditions are incorporated in the scheme of the IIM and in temperature calculations, they are automatically used at each node of the difference mesh for the space variables, including the junction "sphere–cone" in the case of different materials of the spherical and conical parts. The systems of difference equations obtained to determine the temperature in the $n_1$ and $s$ directions were solved by the method of nonmonotonic marching, and for the $\eta$ direction, they were solved by the method of cyclic marching [14] with iterations for the coefficients with the required accuracy.

In each time layer, both the three-dimensional DP and the three-dimensional IP were solved in three steps using the method of splitting in space variables. In the first step, the temperature in the $n_1$ direction was determined. For this, we used a difference scheme obtained by approximation of the derivatives from [6, 7], which gives good results for one-dimensional IP [15]. As a result, to determine the temperature in the $n_1$ direction for any $j$ and $k$, we obtained the recursive relation

$$A_{i+1,j,k}T_{i+2,j,k} + B_{i+1,j,k}T_{i+1,j,k} + C_{i+1,j,k}T_{i,j,k} = D_{i+1,j,k}. \tag{2.1}$$

Here $A_{i+1,j,k} = (F_{1,i+2,j,k} + F_{1,i+1,j,k})/(2h_{n_1}^2) + F_{2,i+1,j,k}/(2h_{n_1})$, $B_{i+1,j,k} = -(F_{1,i+2,j,k} + 2F_{1,i+1,j,k} + F_{1,i,j,k})/(2h_{n_1}^2) - F_{5,i+1,j,k}/h_t + F_{3,i+1,j,k}$, $C_{i+1,j,k} = (F_{1,i+1,j,k} + F_{1,i,j,k})/(2h_{n_1}^2) - F_{2,i+1,j,k}/(2h_{n_1})$, and $D_{i+1,j,k} = -(F_{5,i+1,j,k}/h_t)T_{i+1,j,k}^{m-1} + F_{4,i+1,j,k}$; the subscripts $i$, $j$, $k$, and $m$ correspond to the current node numbers in the difference mesh in the $n_1$, $s$, $\eta$, and $t$ directions ($i = \overline{1,I}$, $j = \overline{1,J}$, $k = \overline{1,K}$, $m = \overline{1,M}$), $h_{n_1}$ and $h_t$ are the sizes of the difference mesh along the variables $n_1$ and $t$, respectively, and $F_1$, $F_2$, $F_3$, $F_4$, and $F_5$ are the coefficients of the heat-conduction equation

$$\frac{\partial}{\partial n_1}\Big(F_1\,\frac{\partial T}{\partial n_1}\Big) + F_2\,\frac{\partial T}{\partial n_1} + F_3T = F_4 + F_5\,\frac{\partial T}{\partial t}, \tag{2.2}$$

whose form is determined by the formulation of the problem. Equations of this form were used to obtain difference schemes of the IIM in the $s$ and $\eta$ directions.

The nonlinear recursive relation (2.1) was used to determine the temperature at the $i$th mesh node from the known temperature at the $(i+1)$th and $(i+2)$th nodes. The temperature obtained at the $i$th node was specified by iterations for the coefficients. The known temperature at the $(i+1)$th node was used as the initial approximation. The computation process began with determining the temperature at the $(I-2)$th node. At the $I$th node, the temperature was specified by the experimental function $T_L^{\exp}(s,\eta,t)$ from (1.11), and at the $(I-1)$th node, it was determined from the finite-difference analog of condition (1.4). Using relation (2.1) for $i = I-2, I-1, \ldots$, and 1 we determined the temperature consistently at all nodes of the difference mesh in the $n_1$ direction for an arbitrary $(j,k)$th beam. The temperature field over the entire shell was determined by employing the above procedure for $j = \overline{1,J}$ and $k = \overline{1,K}$.

In the second step, using the temperature found in the first step as the initial condition in the same time layer, we determined the temperature in the $s$ direction by the IIM. The system of difference equations with a three-diagonal matrix obtained by the IIM for the general equation (2.2) with the most general boundary conditions, including conditions of the first, second, and third kind is given in [13].

In the third step within the time layer considered, we determined the temperature in the $\eta$ direction using the difference scheme of the IIM and the cyclicity condition at $\eta = 2\pi$. The temperature on the rear surface of the shell in the first third of each time layer, used as the boundary condition for calculation of the temperature in the $n_1$ direction, was chosen such the at the end of that time layer, the experimental temperature (1.11) is equal to the calculated temperature obtained upon completion of solution of the IP. Next, we turned to the next time layer and repeated the temperature determination procedure described above. From the temperature field obtained, we determined the total heat flux $Q_w(s,\eta,t)$ and the convective heat flux $q_w(s,\eta,t)$.

The splitting method and the implicit difference scheme of the IIM, which improves the viscosity property of the algorithm of the IP compared to explicit schemes, allow this algorithm to be used over a wide time range to study both fast and long processes of heat transfer. If the error in specifying the initial temperature $T_L^{\exp}(s,\eta,t)$ is such that undesirable oscillations of the solution of the IP arise, it must be smoothed, for example, by means of cubic spline functions [16] or one and two-dimensional cubic V-splines [17] or using the Tikhonov regularization method [18]. If necessary, in the second and third steps, the solution can be regularized. In this case, for the system of difference equations obtained by the IIM, for example in the $s$ direction

$$\begin{gathered} B_{i,1,k}T_{i,1,k} + C_{i,1,k}T_{i,2,k} = D_{i,1,k}, \\ A_{i,j,k}T_{i,j-1,k} + B_{i,j,k}T_{i,j,k} + C_{i,j,k}T_{i,j+1,k} = D_{i,j,k}, \qquad j = \overline{2,J-1}, \\ A_{i,J,k}T_{i,J-1,k} + B_{i,J,k}T_{i,J,k} = D_{i,J,k}, \end{gathered} \tag{2.3}$$

we write the Tikhonov functional

$$\begin{aligned} \Phi_{i,j,k}(\alpha) &= \sum_{j=2}^{J-1} (A_{i,j,k}T_{i,j-1,k} + B_{i,j,k}T_{i,j,k} + C_{i,j,k}T_{i,j+1,k} - D_{i,j,k})^2 \\ &+ (B_{i,1,k}T_{i,1,k} + C_{i,1,k}T_{i,2,k} - D_{i,1,k})^2 + (A_{i,J,k}T_{i,J-1,k} + B_{i,J,k}T_{i,J,k} - D_{i,J,k})^2 \\ &+ \frac{\alpha k_1}{\hbar_{s,j}^2} \sum_{j=1}^{J} (T_{i,j,k} - T_{i,j-1,k})^2 + \frac{\alpha k_2}{\hbar_{s,j}^2} \sum_{j=1}^{J} \Big( \frac{T_{i,j+1,k} - T_{i,j,k}}{h_{s,j}} - \frac{T_{i,j,k} - T_{i,j-1,k}}{h_{s,j-1}} \Big)^2. \end{aligned} \tag{2.4}$$

Here $\hbar_{s,j} = (h_{s,j-1} + h_{s,j})/2$, $h_{s,j}$ are the steps of the variable $s$, $\alpha$ is the regularization parameter, and $k_1$ and $k_2$ are certain nonnegative figures; the coefficients of system (2.3) are given in [13].

After minimization of (2.4) for all $T_{i,j,k}$ $(j = \overline{1,J})$ to determine the temperature in the $s$ direction for fixed $i$ and $k$, as in [6], we obtain a system of nonlinear algebraic equations with a symmetric five-diagonal positive-definite matrix, which is solved by the method of nonmonotonic marching [14] with iterations for the coefficients.

The regularization parameter $\alpha$ is determined by the residual principle

$$\left[ \sum_{m=1}^{M} \sum_{k=1}^{K} \sum_{j=1}^{J} (T_{L,j,k,m} - T_{L,j,k,m}^{\exp})^2 \right]^{0.5} - \delta = 0.$$

Here

$$\delta = \left( \sum_{m=1}^{M} \sum_{k=1}^{K} \sum_{j=1}^{J} \sigma_{j,k,m}^2 \right)^{0.5}$$

is the integral error in specifying the input temperature, $\sigma_{j,k,m}$ is the standard deviation of the error of the function $T_L^{\exp}(s,\eta,t)$ at the nodes of the difference mesh, $T_{L,j,k,m}$ $(j = \overline{1,J},\ k = \overline{1,K},$ and $m = \overline{1,M})$ is the calculated

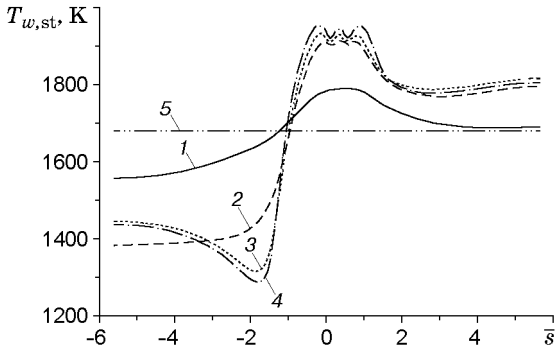


Fig. 2

temperature at the nodes of the difference mesh on the rear surface of the shell obtained by solving the three-dimensional DP with the heat flux $Q_w(T_w)$ on the boundary $n_1 = 0$ found from the solution of the IP.

**3. Results of Numerical Calculations.** The spatial DP was tested by comparison with results of [5], and the IP was tested by comparison with the "exact" solution, i.e., the numerical solution of the spatial DP. Particular program modules, such as the solution of the parabolic equation (2.2), the solution of systems of algebraic equations with three and five-diagonal matrices, etc., were tested employing well-known analytical solutions [13, 14]. A $11 \times 41 \times 13$ computational mesh was used. The time of solution of the reference three-dimensional version of the DP before attainment of the steady-state regime ($t = 200$ sec) was approximately 8 min (the calculations were performed on Pentium-2). The use of a two times finer spatial mesh resulted in a not more than a 0.5% change of the result. In operating with data files, we used one and two-dimensional interpolating and approximating cubic splines. In the boundary layer, we considered a mixed flow regime: laminar flow in the vicinity of the stagnation point on the spherical shell and turbulent flow on the remaining parts of the spherical shell and the cone. The widely used model of point transition from laminar to turbulent flow was used. The transition point $\tilde{s}_*$ was determined such that the sign of the difference in the value of $\alpha/c_p$ between the laminar (1.8) and turbulent (1.9) flows changed with change in $\tilde{s}$ from 0 to $\tilde{s}_1$, and this point depended on the parameters included in formulas (1.8) and (1.9).

Repetition calculations were performed for the determining parameters taken from [5]: $b_1 = 965.5$, $b_2 = 0.147$, $T_{\mathrm{in}} = T_\infty = 300$ K, $c_{p\infty} = 10^3$ J/(kg$\cdot$ K), $L = 0.005$ m, $\varepsilon = 0.85$, $R_N = 0.0185$ m, $\rho_\infty = 0.208$ kg/m$^3$, $V_\infty = 2080$ m/sec, $\beta = 20°$, $\theta = 5°$, $\gamma = 1.4$, $\mathrm{M}_\infty = 6$, and $\mathrm{Pr} = 0.72$.

We considered shell materials with thermal characteristics in a wide range: copper [$\lambda = 386$ W/(m$\cdot$K), $\rho = 8950$ kg/m$^3$, and $c = 376$ J/(kg$\cdot$K)], coal–plastic [$\lambda = 0.75$ W/(m$\cdot$K), $\rho = 1350$ kg/m$^3$, and $c = 1062$ J/(kg$\cdot$K)], and steel [$\lambda = 20$ W/(m$\cdot$K), $\rho = 7800$ kg/m$^3$, and $c = 600$ J/(kg$\cdot$K)]. The pressure distribution on the body surface $p_e/p_{e0}$ was obtained from the solution of the spatial gas-dynamic problem [19].

The solutions of the three-dimensional DP of heat transfer are presented in Figs. 2–4, and those of the IP of heat transfer are presented in Figs. 5 and 6. Figure 2 gives curves of the steady-state ($t = 200$ sec) surface temperature $T_{w,\mathrm{st}}$ versus the $\bar{s}$ coordinate on the windward and leeward sides of the plane of symmetry for copper (curve 1), steel (curve 2), and coal–plastic (curve 3). Curve 4 shows the distribution of the equilibrium radiation temperature $T_{w,\mathrm{eq}}$, which is obtained from the energy conservation equations for the spherical and conical surfaces $q_w = \varepsilon\sigma T_{w,\mathrm{eq}}^4$ and defines the maximum attainable temperature in the absence of heat flow in the longitudinal and circumferential directions. As one might expect, the most intense heat flow occurs for copper, and the least intense heat flow is observed for coal–plastic. For coal–plastic, the steady-state surface temperature differs insignificantly from the equilibrium radiation temperature because the heating of this material is nearly one-dimensional. Because of heat flow along the longitudinal and circumferential coordinates, the steady-state surface temperature for copper far exceeds the on the leeward side and is more than 100 K below the equilibrium radiation temperature on the windward side. For steel, the steady-state surface temperature is different from the radiation equilibrium temperature only on the leeward side, and on the windward side, the difference is negligible. The calculation results for the steady-state regime with $\lambda \to \infty$ show that there is equalization of the temperature profile in the streamline material (straight line 5). The largest value of the steady-state surface temperature for the materials considered is observed in the region of maximum heat flux for turbulent boundary-layer flow near the stagnation point.

In Fig. 2, the steady-state surface temperature for steel on the leeward side of the peripheral part of the cone is below the equilibrium radiation temperature. To explain this effect, we performed numerical calculations

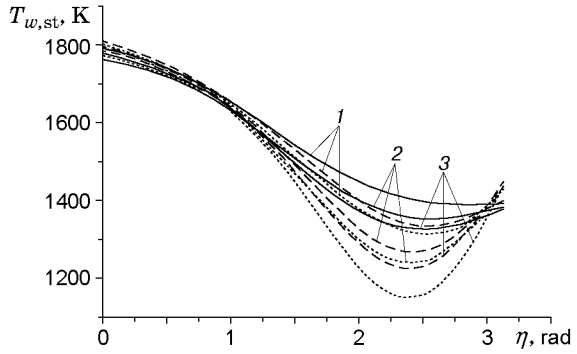


Fig. 3

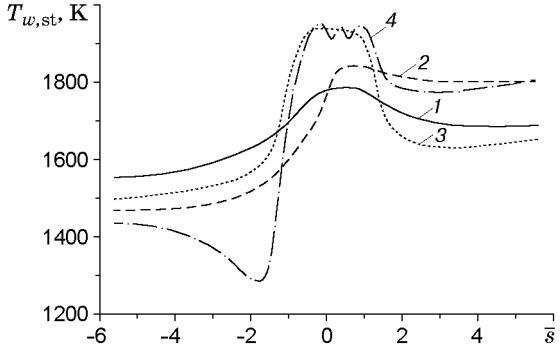


Fig. 4

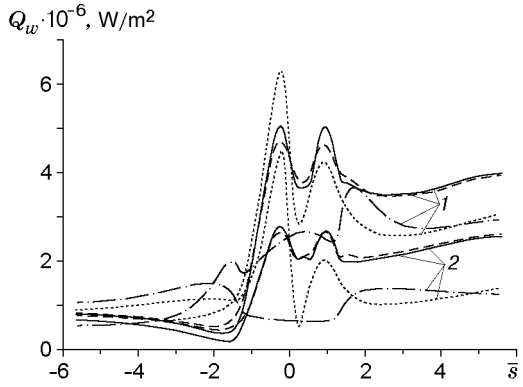


Fig. 5

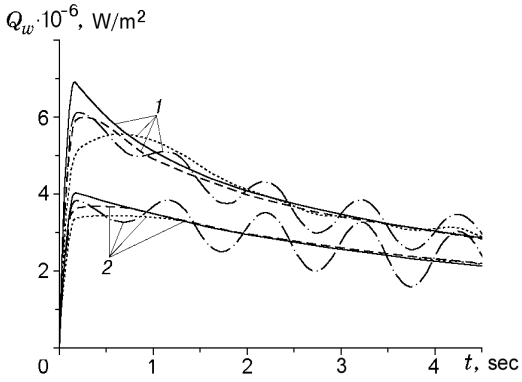


Fig. 6

to determine the temperature in the one- and two-dimensional cases. Figure 3 shows curves of the steady-state surface temperature $T_{w,\mathrm{st}}$ versus $\eta$ for steel at the points with the coordinates $\bar{s} = 3.12$, 4.36, and 5.59 (curves 1–3, respectively). The solid curves are results of solution for the three-dimensional model, the dashed curves are results of solution for the two-dimensional mode, and the dotted curves are solutions for the one-dimensional model. In the steady-state case with the adopted boundary conditions, the temperature obtained for the one-dimensional model coincides with the value of $T_{w,\mathrm{eq}}$. The curve of $T_{w,\mathrm{st}}(\eta)$ on the leeward side of the peripheral part of the cone is nonmonotonic because the heat flux $q_w$ has a minimum on the leeward side at $\eta \approx 2.5$ rad, which is due to the pressure distribution on the outer surface of the boundary layer. This results in a decrease in temperature in this region because of heat flow in the circumferential direction.

The effect of heat flow on heat-transfer was studied numerically for shells made of copper, steel, and coal–plastic. The heating problem was solved in one-, two-, and three-dimensional formulations. It is shown that for a coal–plastic shell, neglect of heat flow along the $\bar{s}$ and $\eta$ coordinates leads to a maximum relative error of 1–2% in determining the steady-state surface temperature, and for a steel shell, this error increases to 5–8% on the leeward side and does not exceed 1–3% on the windward side. The effect of heat flow is most significant for a copper shell. Figure 4 shows curves of $T_{w,\mathrm{st}}(\bar{s})$ for a copper shell in the plane of symmetry obtained with allowance for heat transfer along $n_1$, $\bar{s}$, and $\eta$ (curve 1), $n_1$ and $\bar{s}$ (curve 2), $n_1$ and $\eta$ (curve 3), and $n_1$ (curve 4). As is noted above, curve 4 coincides with the curve of $T_{w,\mathrm{eq}}(\bar{s})$, which is further proof of the validity of the algorithm and the program.

Figure 5 shows the distribution of the total heat flux over the contour in the plane of symmetry at the times $t = 1$ (curves 1) and 5 sec (curves 2) for a copper shell. The solid curves are "exact" solution of the three-dimensional IP and the dashed curves are numerical solutions. Considering the three-dimensionality of the heat-transfer process and the complex nonmonotonic dependence $Q_w(\bar{s})$, the heat flux is reconstructed with fairly high accuracy. The accuracy of reconstructing the steady-state convective heat flux is also high enough. Its maximum value decreases severalfold compared to the initial value and is approximately $1.2 \cdot 10^6$ W/m$^2$. In Fig. 5, the dot-and-dashed curves and dotted curves show the dependence $Q_w(\bar{s})$ obtained from the solution of the one-dimensional IP and the two-dimensional IP, respectively, ignoring heat flow along the circumferential coordinate $\eta$. In all calculation versions,

the initial data for the IP was the "exact " solution of the three-dimensional DP. The step in time in the IP was equal to 0.01 sec. An analysis of Fig. 5 shows that neglect of heat flow along the longitudinal and circumferential coordinates leads to large errors in determining the heat flux. This changes the behavior of the curve of $Q_w(\bar{s})$. The results obtained leads to the conclusion that in reconstructing the heat flux in a shell made of highly heat-conducting materials, one need to use three-dimensional algorithms of the IP.

Figure 6 shows the effect of errors in specifying the initial temperature on the solution of the IP. As an example, the initial temperature specified at ten points in time with a step of 0.5 sec was "disturbed" in time under a saw-tooth law with an amplitude of 1% of its current value. The solid curves show the "exact" dependences of the heat flux on time, the dashed curves are obtained from the solution of the IP with undisturbed initial temperature, and the dot-and-dashed and dotted curves were obtained with disturbed temperature without its preliminary smoothing or regularization of the solution (dot-and-dashed curves) and by smoothing by the Tikhonov regularization method (dotted curves). All time dependences of the heat flux are given in the plane of symmetry at the points with the coordinates $\bar{s} = 0.89$ (curves 1) and $\bar{s} = 1.04$ (curves 2). The results suggest that the proposed algorithm is very effective for solving three-dimensional IP.

Thus, the developed algorithms for solving three-dimensional direct and inverse heat-transfer problems were used to study the effect of heat flow along the longitudinal and circumferential coordinates on heat-transfer characteristics. The effect of thermal conductivity on decrease in the maximum temperatures on the most heat-stressed windward side of the shell of a streamline body was analyzed, and the limits of application of the simplified one- and two-dimensional models to reconstruction of heat fluxes and surface temperatures for highly heat-conducting materials are evaluated.

This work was supported by the Russian Foundation for Fundamental Research (Grant No. 99-01-00352).

## REFERENCES

1. V. A. Bashkin and S. M. , "Calculation of the maximum temperature of a bluntness taking into account the thermal conductivity of the material," *Uch. Zap. TsAGI*, **20**, No. 5, 53–59 (1989).
2. V. A. Bashkin and S. M. Reshet'ko, "Temperature regime of blunted wedges and cones in a supersonic flow with allowance for the thermal conductivity of the wall material," *Uch. Zap. TsAGI*, **21**, No. 4, 11–17 (1990).
3. V. I. Zinchenko, A. G. Kataev, and A. S. Yakimov, "Temperature regimes of streamline bodies with gas injection from a surface," *Prikl. Mekh. Tekh. Fiz.*, No. 6, 57–64 (1992).
4. V. I. Zinchenko, V. I. Laeva, and T. S. Sandrykina, "Calculation of temperature regimes of streamline bodies with various thermal characteristics," *Prikl. Mekh. Tekh. Fiz.*, **37**, No. 5, 106–114 (1996).
5. V. I. Zinchenko and A. S. Yakimov, "Heat transfer characteristics for flow around a spherically blunted cone at incidence and gas injection from a blunted surface," *Prikl. Mekh. Tekh. Fiz.*, **40**, No. 4, 162–169 (1999).
6. V. I. Zinchenko and A. Ya. Kuzin, "Identification of heat-transfer processes for a supersonic flow around a spherically blunted cone using the methods of solving the inverse heat-conduction problems," *Prikl. Mekh. Tekh. Fiz.*, **38**, No. 6, 105–112 (1997).
7. V. I. Zinchenko and A. Ya. Kuzin, "Investigation of heat-transfer processes for a supersonic flow around a spherically blunted cone with allowance for injection of a coolant gas," *Prikl. Mekh. Tekh. Fiz.*, **40**, No. 5, 123–132 (1999).
8. V. I. Zinchenko, *Mathematical Simulation of Conjugate Problems of Heat and Mass Transfer* [in Russian], Izd. Tomsk Univ., Tomsk (1985).
9. O. M. Alifanov, *Inverse Problems of Heat Transfer* [in Russian], Mashinostroenie, Moscow (1988).
10. V. I. Zinchenko and A. Ya. Kuzin, "Investigation of the thermal state of a spherically blunted cone in a hypersonic spatial flow using the methods of solving the direct and inverse problems of heat and mass transfer," in: *Heat and Mass Transfer MMF-2000*, Proc. IV Int. Conf. on Heat and Mass Transfer (Minsk, May 22–26, 2000), Vol. 3, Inst. of Heat and Mass Transfer, National Academy of Sciences of Belarusia (2000), pp. 83–90.
11. B. A. Zemlyanskii and G. N. Stepanov, "Calculation of heat transfer for a spatial hypersonic air flow around thin blunted cones," *Izv. Akad. Nauk SSSR, Ser. Mekh Zhidk. Gaza*, No. 5, 173–177 (1981).
12. N. N. Yanenko, *Method of Fractional Steps for the Solution of Multidimensional Problems of Mathematical Physics* [in Russian], Nauka, Novosibirsk (1967).
13. A. M. Grishin, A. Ya. Kuzin, V. L. Mikov, et al., *Solution of Some Inverse Problems of the Mechanics of Reactive Media* [in Russian], Izd. Tomsk. Univ., Tomsk (1987).
14. A. A. Samarskii and E. S. Nikolaev, *Methods of Solving Mesh Equations* [in Russian], Nauka, Moscow (1978).

15. A. Ya. Kuzin, "Identification of heat- and mass-transfer processes in reactive media," in: *Conjugate Problems of Mechanics and Ecology*, Selected Papers of Int. Conf. (Tomsk, July 4–9, 1998), Izd. Tomsk. Univ. (2000), pp. 190–205.
16. C. H. Reinsch, "Smoothing by spline functions," *Numer. Math.*, **10**, 177–183 (1967).
17. Yu. S. Zav'yalov, B. I. Kvasov, and V. L. Miroshnichenko, *Methods of Spline Functions* [in Russian], Nauka, Moscow (1980).
18. O. M. Alifanov, V. K. Zantsev, B. M. Pankratov, et al., *Algorithms of Diagnostics of Thermal Loads on Flight Vehicles* [in Russian], Mashinostroenie, Moscow (1983).
19. V. A. Antonov, V. D. Gol'din, and F. M. Pakhomov, *Aerodynamics of Airfoils with Injection* [in Russian], Izd. Tomsk. Univ., Tomsk (1990).